J Mater Sci: Mater Electron (2010) 21:692–697
DOI 10.1007/s10854-009-9979-z

The substrate temperature dependent electrical properties of titanium dioxide thin films

A. Yildiz · S. B. Lisesivdin · M. Kasap · Diana Mardare

Received: 4 August 2009 / Accepted: 9 September 2009 / Published online: 19 September 2009

Abstract Titanium dioxide thin films were obtained by a dc sputtering technique onto heated glass substrates. The relationship between the substrate temperature and the electrical properties of the films was investigated. Electrical resistivity measurements showed that three types of conduction channels contribute to conduction mechanism in the temperature range of 13–320 K. The temperature dependence of electrical resistivity between 150 and 320 K indicated that electrical conduction in the films was controlled by potential barriers caused by depletion of carriers at grain boundaries. The conduction mechanism of the films was shifted from grain boundary scattering dominated band conduction to the nearest neighbor hopping conduction at temperatures between 55 and 150 K. Below 55 K, the temperature dependence of electrical resistivity shows variable range hopping conduction. The correlation between the substrate temperature and resistivity behavior is discussed by analyzing the physical plausibility of the hopping parameters and material properties derived by applying different conduction models. With these analyses, various electrical parameters of the present samples such as barrier height, donor concentration, density of states at the Fermi level, acceptor concentration and compensation ratio were determined. Their values as a function of substrate temperature were compared.

A. Yildiz
Department of Physics Faculty of Science and Arts, Ahi Evran University, 40040 Kirsehir, Turkey

A. Yildiz (✉)
Department of Engineering Physics, Faculty of Engineering, Ankara University, 06100 Ankara, Turkey
e-mail: yildizab@gmail.com

S. B. Lisesivdin
Nanotechnology Research Center, Bilkent University, 06800 Bilkent, Ankara, Turkey

M. Kasap
Department of Physics, Faculty of Science and Arts, Gazi University, 06500 Teknikokullar, Ankara, Turkey

D. Mardare
Faculty of Physics, Alexandru Ioan Cuza University, 11 Carol I Blvd, 700506 Iasi, Romania

1 Introduction

Transition-metal oxides are versatile for the design of various electronic devices. This includes e.g., gas sensors, ceramic membrane filters, and spintronic devices to name just a few [1–3]. Among the many possible transition-metal oxides materials, titanium dioxide (TiO_2) is particularly interesting because of its high energy band gap, high refractive index and high dielectric constant [4–7].

There are some recent attempts to understand the outstanding electronic properties of transition-metal oxides [8–10]. However, the picture of electrical transport mechanisms of these materials is not very clear yet, and a more profound understanding is needed. At this stage, a clear understanding of the unique microstructure of grain boundaries enhancing the film conductivity will be prerequisite for practical electronic device application of these materials.

The electrical properties of semiconductors are very sensitive to degree of compensation of the material. Therefore, the determination of the concentration of donors (N_D) and acceptors (N_A) is an important issue. The compensation effects are revealed by the temperature dependence of the apparent carrier concentration deduced by Hall effect measurements. However, the carrier mobility (μ) in TiO_2 being very small ($\mu \ll 1$ cm^2/Vs), the

electrical transport data are limited by the resistivity measurements [9]. Hence, the concentrations of N_D and N_A in TiO_2 thin films generally could not be determined by Hall effect measurements.

One of the possible methods to obtain information on electron transport in transition-metal oxides could be the analysis of temperature dependence of resistivity. Therefore, electron transport properties of TiO_2 thin films can be deeply analyzed with the theoretical calculations which interpret quantitatively the experimental resistivity data. The values of N_D and N_A can also be estimated from temperature dependent resistivity data by correctly identifying the presence of various conduction mechanisms in the material.

As far as we know, the values of N_D and N_A have not yet been directly related to the substrate temperature during deposition of TiO_2 thin films. Therefore, it is important to review and relate these two quantities with substrate temperature (T_s) for extracting conduction mechanism in the context of TiO_2 system. With the detailed investigation of the effects of the substrate temperature on electrical conductivity, it is clear that the various TiO_2 based electronic devices which demands better conductivity may become reliable to produce.

In this paper, we present the relationship between the substrate temperature and the electrical properties of TiO_2 thin films deposited by a dc sputtering technique using water vapour as a reactive gas. The crystallite sizes and system disorder were modified by increasing substrate temperature.

2 Experimental

TiO_2 films were deposited onto heated glass substrates (see Table 1), by a dc sputtering technique. The target to substrate distance was 150 mm, the total pressure being set at 2×10^{-3} mbar. The reactive gas (water vapour) partial pressure was kept constant at 0.6×10^{-3} mbar during the deposition. The deposition rate was 0.03 nm/s. The film thickness, measured by a profilometric method (Alpha-Step 500 Surface Profiler), is the same for the studied samples (280 nm).

X-ray diffraction (XRD) measurements have been carried out with a Rigaku Geigerflex computer-controlled diffractometer, with Cu Kα radiation. The geometry of the diffractometer was the same for all the studied samples (grazing incidence diffraction-5°, U = 40 kV, I = 30 mA) [11]. Figure 1 shows XRD patterns of the investigated samples. The average crystallite sizes (D) have been determined (Table 1), for anatase and rutile phase respectively, from the diffraction peaks A(101), R(110) using the Debye–Scherrer formula:

$$D = \frac{k\lambda}{B_{2\theta}\cos\theta} \quad (1)$$

where k is the Scherrer's constant (k = 0.9), λ is the X-ray wavelength corresponding to CuKα, $B_{2\theta}$ denotes the full-width at half-maximum of the peak and θ is the Bragg angle.

Electrical resistance measurements were performed with a Keithley 196 at temperatures (10–320 K). Two gold rectangular electrodes, placed parallel one to each other at a distance of 0.5 mm, have been used. For temperature dependent resistance measurements, the samples were cooled in a continuous He flow cryostat (Cti-Cryogenics-Helix Technology Corporation, USA) [11].

3 Results and discussion

From the plot of ln(ρ) versus inverse temperature (Fig. 2), one can see that the electrical resistivity of TiO_2 films is influenced by the temperature of the substrate during films deposition. The electrical resistivity measured at room temperature decreases from 1.7 Ωcm for films deposited at T_s = 523 K, to 0.55 Ωcm for those obtained at T_s = 581 K. This could be explained by the improvement in the crystallinity of the films (the increase in the crystallite size, as revealed by XRD data.) with the increase in the substrate temperature. Pure anatase films were obtained at lower substrate temperature (523 K), while a mixed anatase/rutile structure is developed at higher substrate temperature (581 K) (Fig. 1).

As can be seen in Fig. 2, both samples display very similar ρ–T behaviours. The resistivity of the films is found to increase with decrease in temperature and the increase is observed to be very gradual and small for temperatures below certain values. As seen from Fig. 2, no single conduction law can fit the entire curve of the resistivity. From

Table 1 Substrate temperature (T_s), weight percentage of anatase phase (W_A), average crystallite sizes for the anatase phase (D_A) and for rutile phase (D_R), mean crystallite size (L), barrier height (E_b), donor concentration (N_D), Debye screening length (L_D), the experimental NNH activation energy ($W^{exp.}$) and the theoretical NNH activation energy ($W^{teo.}$) with Eq. 10 for the TiO_2 samples

T_s (K)	W_A (%)	D_A (nm)	D_R (nm)	L (nm)	E_b (meV)	N_D (cm^{-3})	L_D (nm)	$W^{exp.}$(meV)	$W^{teo.}$(meV)
581	56	20	12	16	59.6	8.24×10^{18}	3.73	3.5	3.64
523	100	13.9	–	13.9	67.6	6.41×10^{18}	3.04	7.9	6.41

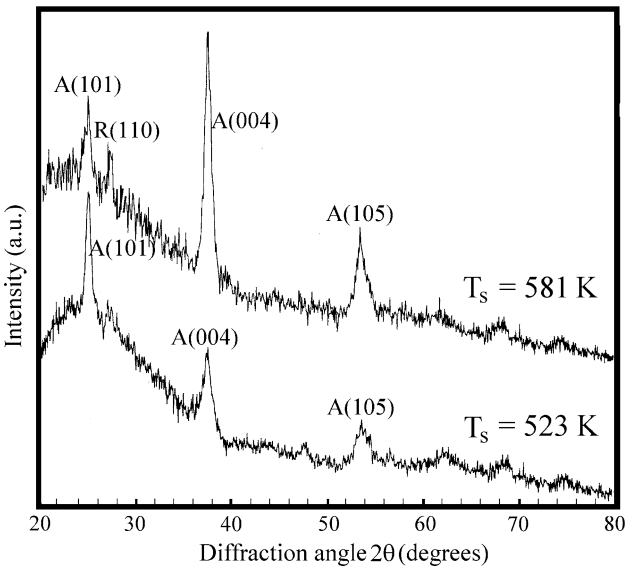

Fig. 1 XRD patterns of studied titanium oxide films

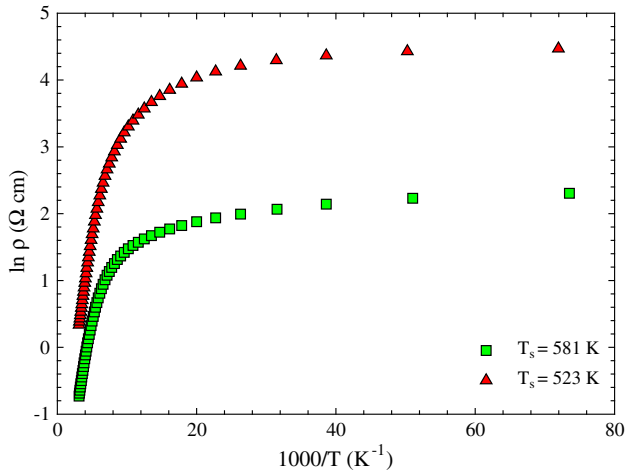

Fig. 2 Temperature dependence of the resistivity plotted as ln(ρ) versus $10^3/T$ in a temperature range 13–320 K

the plots, one may suggest that there are three types of conduction mechanisms contributing to the resistivity in different temperature ranges. These mechanisms may be distinguished experimentally by operating in appropriate temperature ranges, i.e. (i) $T > 150$ K, (ii) $55 < T < 150$ K and (iii) $T < 55$ K.

Since a polycrystalline film has crystallites joined at their surfaces via grain boundaries, the boundaries between crystallites play an important role in determining the conductivity of polycrystalline film. In a polycrystalline material, high densities of defects are expected at the grain boundaries which are often charged with majority carriers. The charged states at the grain boundaries create depleted regions which also act as potential barriers [12, 13]. The XRD measurements indicate that the films obtained at $T_s = 581$ K have larger crystallites than those of the films obtained at $T_s = 523$ K (Table 1). The mean crystallite sizes were calculated as 16 and 13.9 nm for $T_s = 581$ K and $T_s = 523$ K, respectively. As the substrate temperature decreases, the crystallite size decreases and this leads to an increment in the trapping states at grain boundary. Trapping states are capable of trapping free carriers and, as a consequence, more free carriers become immobilized as the trapping states increases. On the other words, the larger crystallite size results in a lower density of grain boundaries, which behave as traps for free carriers and barriers for carrier transport in the film. Hence, an increase in the crystallite size can cause a decrease in grain boundary scattering, which leads to a decrease in the resistivity.

At high temperatures, the temperature dependence of electrical resistivity for polycrystalline films was analyzed by the grain boundary model [12, 13]. Therefore, in the present samples, resistivity (ρ) of thermally activated band conduction can be expresses by grain boundary model for the $T > 150$ K. The electrical resistivity can be expressed as [12],

$$\rho = \left(\frac{(2\pi m^* \mathrm{k_B T})^{1/2}}{L\mathrm{e}^2\mathrm{n}}\right) \exp\left(\frac{E_b}{\mathrm{k_B}T}\right) \tag{2}$$

where e is the electron charge, n is the electron concentration in neutral region of crystallites, L is the mean size of the crystallites, k_B is the Boltzmann's constant, m^* is the effective mass of charge carriers and E_b is the barrier energy at boundary which can be described as [12],

$$E_b = \frac{L^2 e^2 N_D}{8\varepsilon} \tag{3}$$

where ε is the low frequency dielectric constant. For samples deposited at $T_s = 581$ K, which contain anatase phase in proportion of 56%, the calculated dielectric constant (ε) can be taken as about 80 [14]. For other, 100% anatase phase sample which is deposited at $T_s = 523$ K, ε is about 41.4 [14]. As mentioned earlier, applicability of grain boundary model involve many grain boundaries. This effect is examined by evaluation of the Debye screening length (L_D) in comparison with the mean crystallite size (L). L_D is given as [13],

$$\mathrm{L}_D = \sqrt{\mathrm{k_B} T \varepsilon_0 \varepsilon / \mathrm{e}^2 N_D} \tag{4}$$

where ε_0 is the dielectric constant of vacuum. If $L_D < L/2$, potential barriers exist in grain boundary region due to interface trap states [13]. If, however, L_D is larger than $L/2$, the conduction band becomes flat without the potential barrier [13], and the electrons are transported without grain boundary scattering.

In Fig. 3, the linear part in the investigated temperature range indicates the grain boundary scattering of the charge

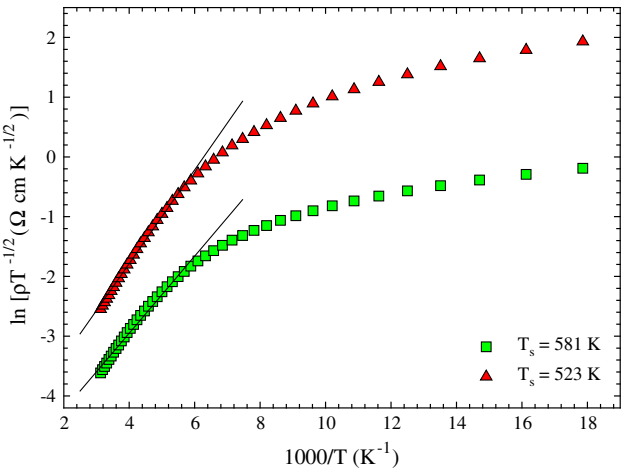

Fig. 3 Temperature dependence of the resistivity plotted as $\ln(\rho T^{-1/2})$ versus $10^3/T$ in a temperature range 55–320 K. *Solid lines* are the best-fit lines with Eq. 2

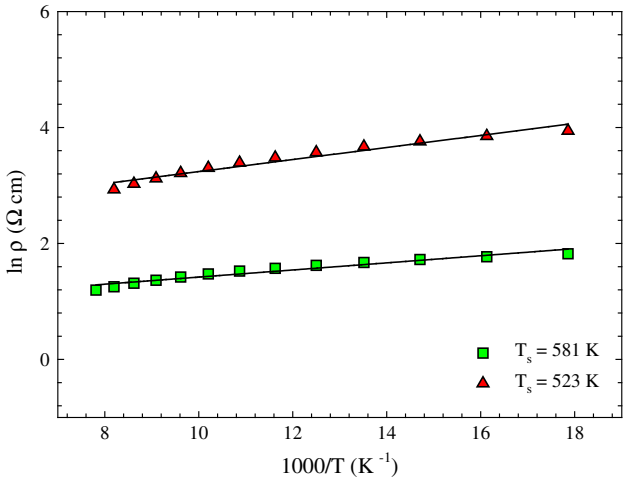

Fig. 4 Temperature dependence of the resistivity plotted as $\ln(\rho)$ versus $10^3/T$ in a temperature range 55–130 K. *Solid lines* represent the best-fit lines with Eq. 9

carriers is the predominant mechanism in the films. The potential barrier height of the films (E_b) was calculated from the slope of the curves of Fig. 3. The potential barrier height of the films decreased from 67.6 to 59.6 meV with the increase of substrate temperature from 523 to 581 K, respectively. The decrease of potential barrier height with the increase of substrate temperature is due to the increase of crystallite size resulting in the decrease of the scattering of charge carriers at the grain boundaries.

The values of the donor carrier concentration (N_D) and Debye screening length (L_D) can be calculated with the previously obtained values of E_b and L. The calculated values of N_D and L_D are given in Table 1. With an increase of the substrate temperature, N_D increases. It can be noticed that the condition $L_D < L/2$ is obeyed for both sample. This condition is appropriate for a grain boundary model. Thus, the approach of analyzing the data using the grain boundary model for the thermal activation of conductivity is valid for both samples in a temperature range of 150–320 K.

Deviations from the linearity in the temperature dependence of the resistivity (Fig. 3) cannot be explained by band conduction at temperatures below 150 K. Therefore, another conduction model should be taken into account. For *n*-type semiconductors, most of the free electrons are recaptured by the donors at low temperatures. Then the electrons have not sufficient energy to jump from donor levels to conduction band [15]. In this case, the band conduction becomes less important, and electron hopping directly between donor states in the impurity band will bring the main contribution to the conduction mechanism [15, 16]. When these impurity centers are partially compensated, hopping conduction becomes possible. Since TiO_2 has the high band gap energy and small Bohr radius, it is possible to observe hopping conduction at relatively high temperatures [17].

By plotting $\ln(\rho)$ versus $1000/T$ in Fig. 4 for temperature range of 55–150 K, a linear relationship is obtained particulary in a temperature range 55–125 K and 55–130 K for the films deposited at $T_s = 523$ K and at $T_s = 581$ K, respectively. The estimated activation energies at this temperature region have much smaller values as compared to the energy (E_b) required for thermally activated band conduction. This suggests that the electrical conduction in the films is dominated by a hopping conduction which is called as nearest-neighbor hopping (NNH) conduction mechanism [15]. In the NNH conduction, electron hops to the nearest neighbor empty site. For the localized states with an energy separation W and the NNH distance r, the hopping probability can be written as [15, 16].

$$P_{hop} = v_{ph} \exp(-2r/\xi - W/k_B T) \tag{5}$$

where v_{ph} is the phonon frequency associated with hopping process, and ξ is the localization length. The diffusion coefficient D_{hop} for hopping is given by [15, 16]

$$D_{hop} = P_{hop} r^2/6. \tag{6}$$

Using the Einstein relation, the resistivity can be written as

$$\rho = \frac{1}{e^2 D_{hop} N(E_F)}. \tag{7}$$

Combining Eqs. 5–7, the temperature dependence of resistivity in the NNH regime is found as [15, 16]

$$\rho = \left[\frac{1}{6} N(E_F) v_{ph} e^2 r^2\right]^{-1} \exp(2r/\xi + W/k_B T) \tag{8}$$

$$\rho = \rho_3 \exp(W/k_B T) \tag{9}$$

where $(N(E_F))$ is the density of states (DOS) and W is defined as the average energy needed to hop to the nearest

neighbor at a distance r. From simple potential considerations W would be estimated using the following equation [18]

$$W = \frac{0.99e^2 N_D^{1/3}}{4\pi\varepsilon}. \quad (10)$$

Utilizing the values of N_D obtained from Eq. 3, the theoretical values of W are obtained by Eq. 10. As seen from Table 1, these theoretical values of W are in good agreement with extracted experimental values from the slopes of the curves in Fig. 4. Hence, one can expect that the determined values of N_D are correct for both films.

With the decreasing temperature, the spatial term in Eq. 5 begins to affect the resistivity. When the phonon energy is insufficient, the more energetic phonon-assisted hops becomes favorable, as a result of which the electrons will tend to hop larger distance in order to locate sites which are energetically closer than the nearest neighbors. This new regime is known as Mott variable range hopping conduction (VRH) regime [19]. Below a certain critical temperature the hopping process changes from NNH to VRH, where the carrier jumps between more remote defect centers which are close in energy. The critical temperature for transition from NNH to VRH proposed by Pollak [20] is determined by

$$T_c = 5.2e^2 N_D^{2/3} \xi / k_B (4\pi\varepsilon\varepsilon_0). \quad (11)$$

Taking the value of 8.06 Å for ξ [21], the values of the critical temperature for transition from NNH to VRH are determined. These values are collected in Table 2. It is obvious from Table 2 that the value of critical temperature decreases with increasing substrate temperature. The theoretical finding is consistent with the experimental observations. As seen from Fig. 2, the weak temperature dependence of the resistivity for $T < 55$ K shows that the conduction mechanism is possibly dominated by VRH conduction mechanism instead of thermal excitation. The difference between theoretical and experimental values of critical temperature for transition from NNH to VRH may be due to uncertainties in estimating the values of ξ and ε.

In the VRH conduction case, the resistivity should follow the law [19],

Table 2 The critical temperature (T_c) for transition from NNH to VRH, characteristic hopping temperature (T_0), density of states at Fermi level $N(E_F)$, acceptor concentration (N_A), compensation ratio (N_A/N_D) for the TiO_2 samples

T_s (K)	T_c (K)	T_0 (K)	$N(E_F)$ (cm^{-3} eV^{-1})	N_A (cm^{-3})	N_A/N_D
581	36	7.32×10^3	5.44×10^{22}	9.91×10^{17}	0.121
523	58	9.75×10^3	4.09×10^{22}	1.32×10^{18}	0.206

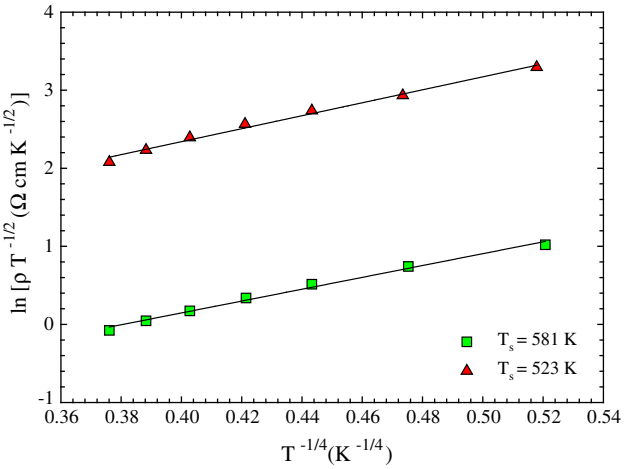

Fig. 5 Temperature dependence of the resistivity plotted as $\ln(\rho T^{-1/2})$ versus $T^{-1/4}$ in a temperature range 13–55 K. *Solid lines* represent the best-fit lines with Eq. 10

$$\rho = \rho_0 T^{1/2} \exp\left[\left(\frac{T_0}{T}\right)^{1/4}\right], \quad (12)$$

where

$$\frac{1}{\rho_0} = \frac{3e^2 v_{ph}}{(8\pi)^{1/2}} \left[\frac{N(E_F)\xi}{k_B}\right]^{1/2}. \quad (13)$$

We have fitted our data for $T < 55$ K in the VRH model. Figure 5 shows the fitting. Good linearity at considered temperature range confirms VRH conduction for both films, even though the films are deposited at different substrate temperature. The values of T_0, obtained from the slope of the curves of Fig. 5, are given in Table 2. Using these T_0 values, the density of states at the Fermi level, $N(E_F)$, have been estimated using the relation [19],

$$T_0 = \frac{18}{k_B N(E_F)\xi^3}. \quad (14)$$

Estimated values of $N(E_F)$ are also collected in Table 2. The estimated values of $N(E_F)$ are the same orders of magnitude as reported for TiO_2 [8, 22].

The hopping conduction can be fulfilled only by donor–acceptor compensation at low temperatures. We can now obtain the acceptors concentration (N_A) using an expression valid for a compensated material [18];

$$N(E_F) = (2\varepsilon/e^2) N_A N_D^{-1/3}. \quad (15)$$

Substituting the values of $N(E_F)$ and N_D into Eq. 15, the values of N_A and then compensation ratio N_A/N_D are determined. Their values are collected in Table 2. An increasing in the compensation ratio results in an increase in resistivity of TiO_2 thin films. If a system is very lightly compensated ($N_A/N_D \ll 0.1$), its relatively small average binding energy allows only excitation to the conduction band

at low temperatures [23]. Therefore, the VRH conduction mechanism will be dominant at only low temperatures for very lightly compensated systems. On the other hand, as the compensation ratio increases, the relatively large average binding energy allows only excitation to the conduction band at relatively high temperatures [23]. Therefore, VRH conduction mechanism will be dominant at even high temperatures ($13 < T < 55$ K). The increase in compensation ratio reflects the value of T_0. From Table 2, one can observe a decrease in the value of T_0 with the increase in substrate temperature. Since the value of T_0 is a measure of disorder in the material, the increase in the substrate temperature results in a decrease in disorder of the films [18, 19]. The only adjustable parameter in Eq. 14 which might be affected by the substrate temperature is $N(E_F)$. A higher substrate temperature may be expected to lead to an increase in $N(E_F)$. If so, a decrease in T_0 is expected as the substrate temperature is increased.

4 Conclusion

TiO_2 thin films were obtained by a dc sputtering technique onto glass substrates. The effect of substrate temperature on the electric properties was investigated by studying of the electrical resistivity in a temperature range of 13–320 K. The electrical analyses results show three types of conduction channel that contribute to conduction mechanism. Due to the decrease in substrate temperature, almost all the physical parameters of interest have consequently changed. It was found that the crystallinity decreases with decrease in substrate temperature. The limiting factor governing this change in the physical parameters of the film is the crystallite size, which decreases with decreasing substrate temperature. This decrease in the crystallite size determines the increase of defect states. Due to the decrease in substrate temperature and hence, potential barrier height, the resistivity, characteristic hopping temperature and compensation ratio have increased. Various electrical parameters of the present samples are found to be appropriate for various conduction models.

Acknowledgements One of the authors (D. Mardare) is very indebted to Professor F. Levy from Institute of Applied Physics, Polytechnic Federal School of Lausanne, Switzerland for providing the necessary laboratory facilities to carry out a part of this investigation. This work was supported by TUBITAK and ANCS under project nos TBAG-U/220 (107T584) and 17CB/06.06.2008. Abdullah Yildiz acknowledges 2218 coded national research scholarship from BİDEB.

References

1. D. Mardare, N. Iftimie, D. Luca, J. Non-Cryst. Solids **354**, 4396 (2008)
2. Y. Yao, G. Li, K.A. Gray, R.M. Lueptow, Langmuir **24**, 7072 (2008)
3. Y. Matsumoto, M. Murakami, T. Shono, T. Fukumura, M. Kawasaki, P. Ahmet, T. Chikyow, S. Kohsihara, H. Koinuma, Science **291**, 854 (2001)
4. D. Mardare, M. Tasca, M. Delibas, G.I. Rusu, Appl. Surf. Sci. **156**, 200 (2000)
5. D. Mardare, Mater. Sci. Eng. B **95**, 83 (2002)
6. D. Mardare, P. Hones, Mater. Sci. Eng. B **68**, 42 (1999)
7. D. Mardare, G.I. Rusu, J. Opt. Adv. Mater. **6**, 333 (2004)
8. A. Yildiz, S.B. Lisesivdin, M. Kasap, D. Mardare, J. Non-Cryst. Solids **354**, 4944 (2008)
9. A. Yildiz, S.B. Lisesivdin, M. Kasap, D. Mardare, Physica B **404**, 1423 (2009)
10. B.V. Kumar, T. Sankarappa, M.P. Kumar, S. Kumar, J. Non-Cryst. Solids **355**, 229 (2009)
11. D. Mardare, G.I. Rusu, Phys. Low-Dimens. Struct. **11/12**, 69 (1999)
12. J.Y.W. Seto, J. Appl. Phys. **46**, 5247 (1975)
13. J.W. Orton, M.J. Powel, Rep. Prog. Phys. **43**, 1263 (1980)
14. J.Y. Kim, H.S. Jung, J.H. No, J.R. Kim, K.S. Hong, J. Electroceram. **16**, 447 (2006)
15. A. Miller, E. Abrahamas, Phys. Rev. **120**, 745 (1960)
16. R.A. Street, *Hydrogenated Amorphous Silicon* (Cambridge University Press, Cambridge, 1991)
17. H. Tang, K. Prasad, R. Sanjines, P.E. Schmid, F. Levy, J. Appl. Phys. **75**, 2042 (1994)
18. B.I. Shklovskii, Sov. Phys. Semicond. **6**, 1053 (1973)
19. N.F. Mott, E.A. Davis, *Electronic Properties in Non-Crystalline Materials* (Clarendon Press, Oxford, 1971)
20. M. Pollak, Philos. Mag. B **42**, 781 (1980)
21. S. Mahadevan, A. Giridhar, K.G. Rao, J. Phys. C **10**, 4499 (1977)
22. A.K. Hassan, N.B. Chaure, A.K. Ray, A.V. Nabok, S. Habesch, J. Phys. D **36**, 1120 (2003)
23. M. Benzaquen, D. Walsh, K. Mazuruk, Phys. Rev. B **36**, 4748 (1987)